LHCb Note 2004-106

Radiation Damage and Cooling Requirements for the LHCb Inner Tracker

S. Koestner, H. Voss

December 3, 2010

Abstract

Simulations of radiation levels in the LHCb experiment are used to study the impact of radiation damage on the LHCb Inner Tracker. The expected performance of the silicon detectors after irradiation damage is addressed. Furthermore, the results are used to define the respective cooling requirements for the silicon modules to ensure 10 years of operation of the detector.

Disclaimer: Despite the publication date, this is an old note with old calculations done in 2004. I apologize for the late publishing.

1 Introduction

The "Inner Tracker" [1] is part of the LHCb [2] tracking system. There are three tracking stations located behind the bending magnet. The "Inner Tracker" covers the high particle density region close to the beam-pipe with silicon micro-strip detectors. The outer region is covered by the "Outer Tracker" which is designed as a straw tube detector.

The Inner Tracker consists of 4 individual detector boxes per station, which are arranged around the beam-pipe. There are 4 detection layers per station. The boxes placed at the sides of the beam-pipe host modules built out of two silicon sensors bonded together to form a 22 cm long detector, while the modules above and below the beam-pipe consist of one single sensor only. The silicon thickness is 410 μm for the 22 cm long modules and 320 μm for the short 11 cm single sensor modules. The sensor strip geometry is given by a pitch of 198 μm and an implant width of 50 μm.

The detector boxes of the individual stations will be placed as close as possible (respecting a 7 mm security margin) to the beam-pipe. Due to the conical shape of the beam-pipe, this results in a closest position of the start of the sensitive area of the silicon detectors w.r.t. the center of the beam-pipe of 92.5 mm, 99.5 mm and 106.5 mm for the Inner Tracker stations IT1, IT2 and IT3, respectively[1]. Being close to the beampipe, the

[1]These numbers refer to the start of the sensitive detector area, excluding the 1 mm guard rings on the silicon sensor.

detectors are subject to substantial radiation during the LHC operation. The radiation background in the LHCb experiment has been simulated with FLUKA [3] and is documented in [4]. We use these simulations to estimate the radiation damage expected for the Inner Tracker silicon modules after 10 years of operation, corresponding to $1.6 \cdot 10^{15}$ pp-collisions.

The radiation profile and the resulting leakage currents expected in the silicon detectors are given in section 2. In section 3 the expected S/N after irradiation is estimated as a function of possible operating temperatures. The impact of the radiation damage on the effective doping concentration and hence the depletion voltage is given in section 4 and finally the cooling requirements with respect to thermal run-away are addressed in section 5. The detector design, which ensures the fulfillment of these requrirements is presented in a seperate note [5].

2 Particle fluences and leakage current

The two dimensional radiation map of the estimated particle flux in 1 MeV neutron equivalent/cm^2 after 10 years of LHC operation as it will be seen in the region of the Inner Tracker is show in figure 1. The radiation levels close to the beam-pipe reach up to approximately $\approx 1 \cdot 10^{13}$ 1 MeV neutron equivalent/cm^2. In figure 2, the fluxes are averaged over vertical regions

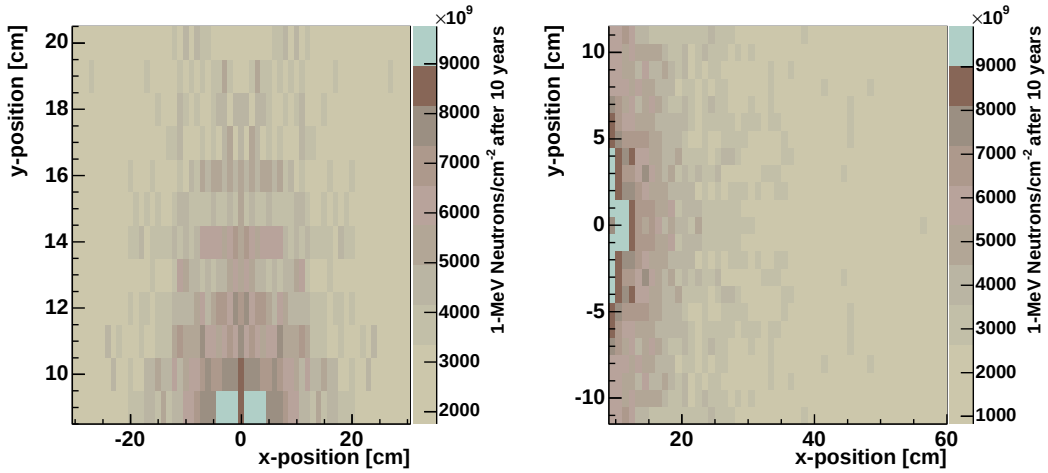

Figure 1: The expected integrated particle flux in 1 MeV neutron equivalent / cm^2 after 10 years of LHC operation in the area covered by a top/bottom detector box (left) and a side detector box (right).

(y-axis) from 0 cm to 5 cm for the side boxes and 10 cm to 15 cm for the top/bottom boxes. For each point on the horizontal x-axis, this y-region corresponds to the part of the silicon that recieves the highes radiation dose in the respective detector boxes. Particle fluxes of up to $0.9 \cdot 10^{13}$ 1 MeV neutron equivalent/cm^2 are found for the side box while the maximum reached for the top/bottom boxes is about $0.7 \cdot 10^{13}$ 1 MeV neutron equivalent/cm^2

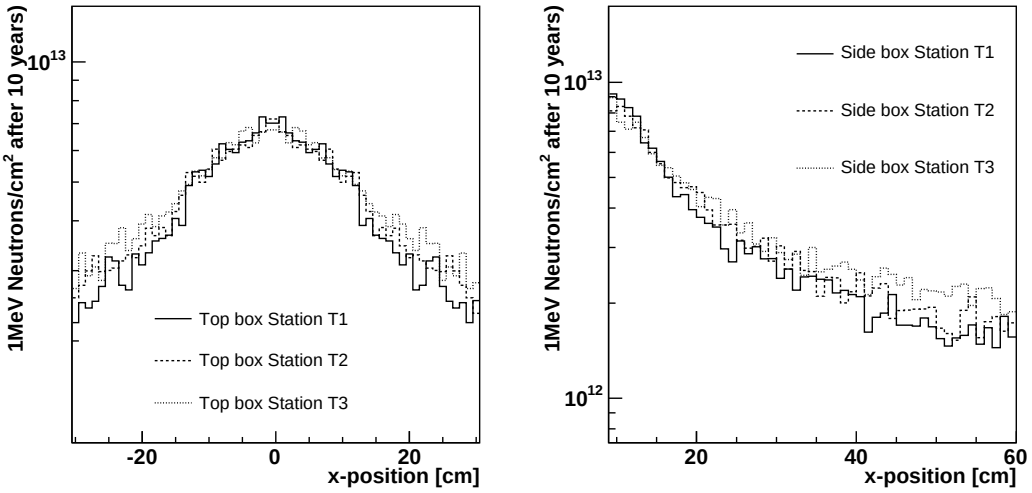

Figure 2: The expected integrated particle flux in 1 MeV neutron equivalent/cm^2 after 10 years of LHC operation. The fluxes are averaged over vertical regions (y-axis) from 0 cm to 5 cm for the side boxes and 10 cm to 15 cm for the top/bottom boxes. For each point on the horizontal x-axis, this y-region corresponds to the part of the silicon that recieves the highes radiation dose in the respective detector boxes.

The radiation causes bulk damage in the silicon and hence results in an increased leakage current. This leakage current has been shown to be proportional to the integrated flux according to the relation [6]:

$$I_{leak} = \alpha \cdot \Phi \cdot V \qquad @\, 20^\circ C, \tag{1}$$

where $\alpha = 4 \cdot 10^{-17}\mathrm{A\,cm^{-1}}$ is the radiation induced damage constant for 1 MeV neutrons, Φ is the particle flux in 1 MeV neutron equivalent/cm^2 and V is the irradiated silicon volume. The expected leakage current at the position of the different readout strips in the detector after the irradiation is shown in figure 3. The increased leakage currents need to be controlled as they have two main negative effects. They result in increased shot noise and hence a degradation of the detector performance and second they result in a significant power dissipation in the sensors, which needs to be removed. The leakage currents can be decreased if the detectors are cooled. The exponential dependence of the leakage current on the silicon bulk temperature is given by:

$$\frac{I_{leak}(T_1)}{I_{leak}(T_2)} = \left(\frac{T_1}{T_2}\right)^2 \cdot \exp\frac{E_g(T_1 - T_2)}{2k_B T_1 T_2}\ ; \tag{2}$$

where $E_g = 1.2\mathrm{eV}$ is the band gap for silicon and $k_B = 8.6 \cdot 10^{-5}\mathrm{eV/K}$ is the Boltzmann constant. This results in a leakage current that decreases by a factor two for approximately every $7^\circ C$.

The power dissipation in the silicon can be calculated using the thermally generated leakage current and the applied bias voltage (P=U·I). In figure 4 this power dissipation is shown for each module for an operating

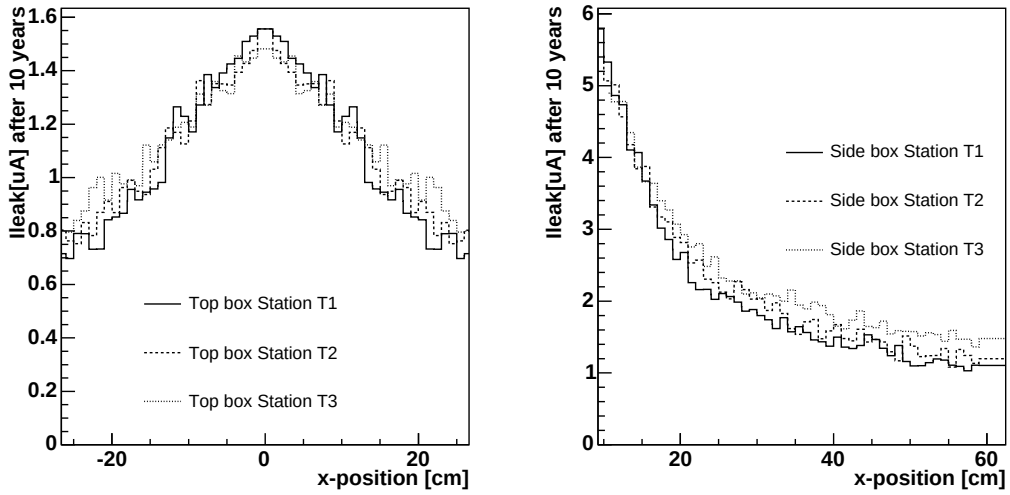

Figure 3: The expected leakage current at $20^\circ C$ per strip in the silicon sensors after 10 years of operation.

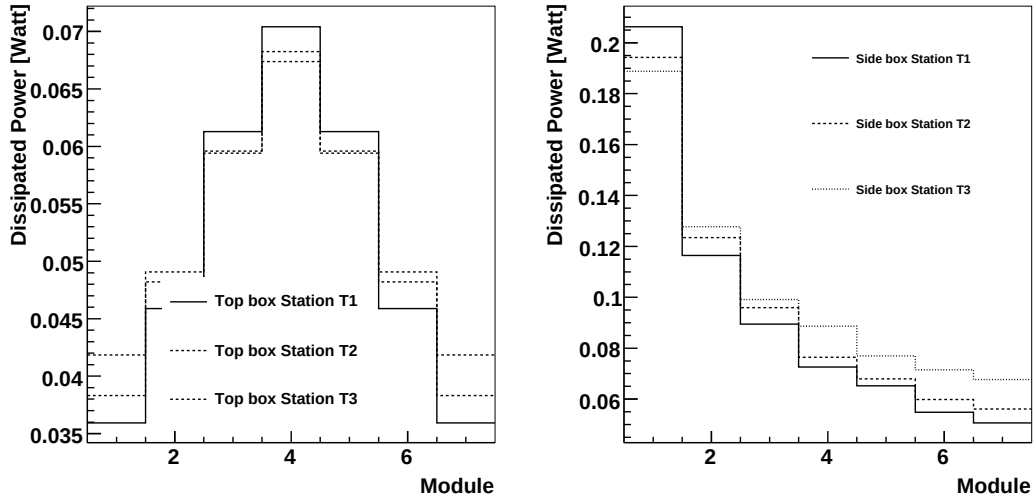

Figure 4: The power dissipation in the various modules at $10^\circ C$ after 10 years of operation as a function of the silicon bulk temperature for a bias voltage of 300V.

temperature of $10^\circ C$ of the silicon sensors, and an assumed bias voltage of 300 V.

The overall heat flow into the detector box is estimated from the three sources: the Beetle readout chips, the heat flow throught the box walls and the power dissipation in the silicon sensors. Each readout chip has a power consumption of 0.86W under normal running conditions and triggerd at 1MHz, which amounts to a total of 3 Beetles/module $\cdot$ 28 modules/box $\cdot$ 0.86 Watt = 72.24 Watt. The heat flow through the box walls can be estimated from the temperature difference between the outside and the inside of the box together with the thermal resistivity of the box walls which has been measured to 2.2-2.4W/(m$^2 \cdot$ K) [13]. The result of this is shown in figure 5, assuming a temperature in the experimental hall of

$22\,^{\circ}C$. For these estimates, it is assumed that the silicon bulk (biased at 300 V) temperature is $5^{\circ}\,C$ higher temperature than the ambient air. It can

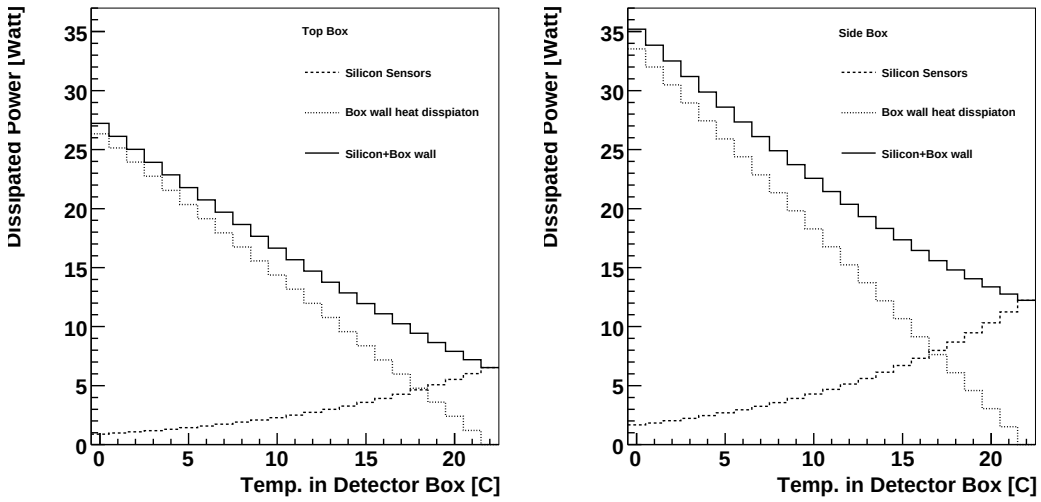

Figure 5: The power dissipation into the detector box from the silicon sensors (operating $10^{\circ}\,C$ after 10 years of operation) and through heat conduction through the walls as a function of the ambient air temperature.

clearly be seen, that with the present insulation of the detector boxes, the reduction of power dissipation in the sensors for lower box temperatures is overcompensated by the larger heat flow through the boxe walls. However, both the heat flow through the box walls and the sensors are considerably smaller than the power dissipation in the readout chips. Together with the readout chip power dissipation, a total of approximately 100 W needs to be removed from each detector box.

3 Detector performance

The detector performance before irradiation can be estimated from test-beam [10] results and extrapolations to the final sensor geometries, in a very similar way as also performed already for the TT-station [11]. A good understanding of the S/N performance in terms of the generated signal and the expected noise due to the capacitive load which the sensor represents for the pre-amplifier has been obtained. A generated signal charge of 25040 e^- and 32640 e^- as the most probable value in the Landau distribution is expected for 320 μm and 410 μm think sensors, respectively. The Beetle pre-amplifier noise dependence on the load capacitance as obtained in lab measurements is given by:

$$ENC = 540\,e^- + 49\,e^-/\mathrm{pF} \cdot C_{strip} \quad @V_{fs} = 400\mathrm{mV} \tag{3}$$

This expectation was tested with test-beam data from various detectors having different strip capacitances, strip lengths and sensor thicknesses. Agreement was reached under the assumptions that the expected charge is the one collected at the central strip of the detector and no further strip

length dependent noise sources, like for example the readout strip resistance, were considered as attributing to the noise. An additional constant noise source, attributed to the test-beam setup, resulted in a larger offset of some 776 e^- compared to the 540 e^- from the lab measurements. This larger number will be used as the pessimistic estimate of the detector performance. The strip capacitance for the sensors used in the top/bottom boxes has been measured to 1.41 pFcm^{-1}, with an additional 2 pF from the pitch-adapter. The sensors in the side boxes employ the same strip geometry but have a larger thickness, which should result in a smaller strip capacitance. For a conservative estimate, the same value for the strip capacitance as for the thinner sensors will be used here. This results in:

strip length :	11 cm	22 cm
load capacitance :	17.5 pF	33 pF
ENC :	1398 e^-	2060 e^-
S/N :	17.9	15.8
ENC (pessimistic) :	1634 e^-	2296 e^-
S/N (pessimistic) :	15.3	14.2

Using the leakage current increase according to the formula 1 and its temperature dependence according to formula 2, the expected S/N performance of the detector after irradiation can be estimated. This estimation assumes, that the only effect of the irradiation is through the increased shot noise due to the leakage current according to:

$$\mathrm{ENC}_{I_{leak}} = \sqrt{12 \cdot I_{leak}[nA] \cdot \tau[ns]}\ ; \qquad (4)$$

where τ is the rise-time of the pulse-shape, which is approximately 15 ns for a Beetle setting of V_{fs}=400 mV. For 4 times larger radiation, a possible 15% increase in the total strip capacitance has been observed in our test measurements [7] and also reported by other experiments [9]. No measurable increase in the strip capacitance has been observed for the nominal flux expected for the LHCb Inner Tracker. Hence a strip capacitance after irradiation of 1.62 pF/cm is used together with the "pessimistic" scenario in order to form a "very pessimistic" estimate.

ENC (very pessimistic) :	1747 e^-	2620 e^-
S/N (very pessimistic) :	14.3	12.5

A 20% decrease in the charge collection efficiency might be expected, for particle fluxes 10 times as high as for the Inner Tracker. Test-beam measurements with irradiated sensors according to 10 years of operation of the LHCb did not show any inefficiency in the charge collection and hence this effect can be neglected. The result of the S/N estimates as a function of the operating temperatures is shown in figure 6. This estimate shows, that the increase in noise due to the larger leakage current present at slightly elevated temperatures, doesn't cause a problem for the obtained S/N values. We typically have full detection efficiency with acceptable noise rates for a S/N above 10-11, which is comfortably reached for all operating temperatures. This holds true even for the S/N values expected in between two readout strips, where we typically loose 15% of the generated charge.

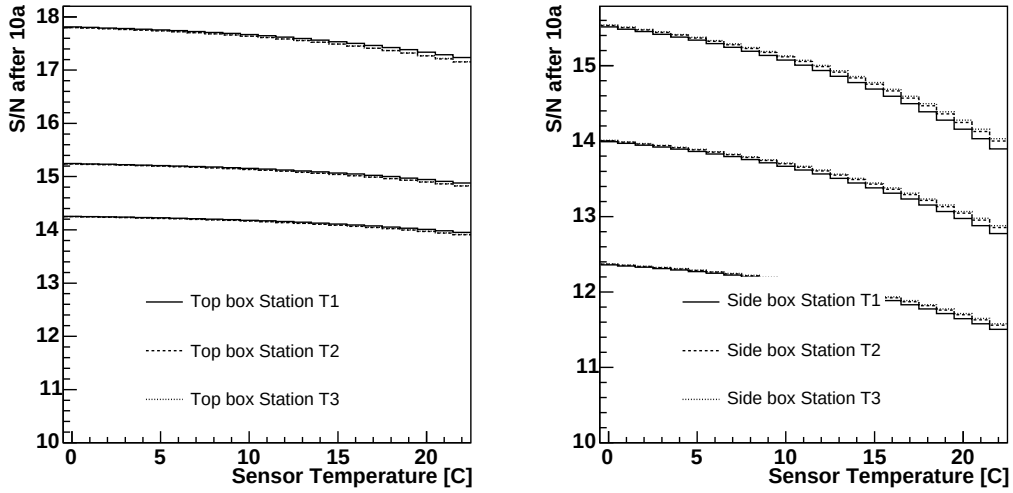

Figure 6: The expected S/N performance of the detector dependent on the operating temperature after 10 years of operation. In each plot, the upper lines correspond to the optimistic approach using the lab measurements of the Beetle performance, the middle curves correspond to the values closer to the test-beam while the curves at them bottom simulate the very pessimistic scenario assuming also an additional 15% strip capacitance increase due to the irradiation.

4 The depletion voltage

The depletion voltage in silicon sensors is determined by the effective dopant concentration of the bulk material. The radiation damage leads to a steady decrease of the initial n-doping until at some point the bulk becomes intrinsic. Afterwards, the bulk becomes effectively p-type. Accordingly, the depletion voltage first falls off to zero and then rises again. The fluence dependent depletion voltage of silicon sensors has been investigated and modeled [8] in the so called "Hamburg model", which takes into account stable damage, short-term beneficial annealing as well as long-term reverse annealing. For our standard float-zone silicon detectors with 410 μm thickness and a specified initial resistivity of 4-9k$\Omega \cdot$cm the results of the expected depletion voltage are given in figure 7. In this calculation, an safety factor of 2 in the expected radiation dose is assumed, leading to a maximum fluence of $2 \cdot 10^{13}$-neutron equivalent/cm^2 after 10 years of operation close to the beam-pipe. The final depletion voltage depends on the operating temperature and the warm up scenarios, as these influence the beneficial and reverse annealing. In all cases, the final depletion voltage doesn't exceed 100 V. For full charge collection, a significant over-depletion is necessary and therefore an operating voltage of 300 V is assumed throughout this note to account for a safety margin in all the power calculation.

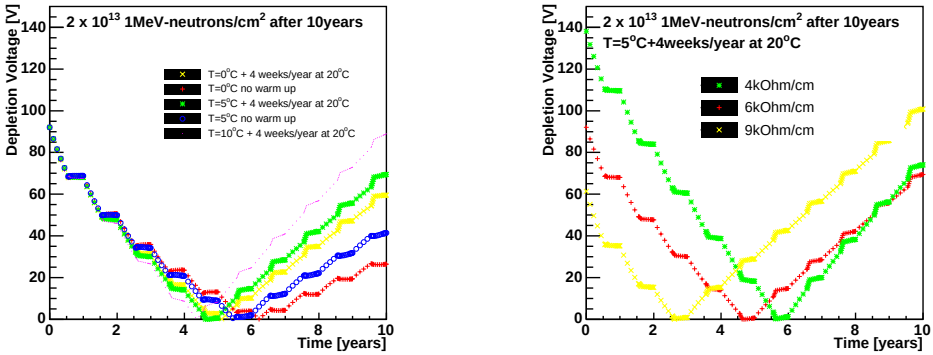

Figure 7: The expected depletion voltage of the 410 μm thick sensors as a function of time (fluence) for different scenarios of temperatures (left) and initial effective doping reflected by the depletion voltage.

5 Thermal energy balance

An important aspect in the operation of silicon sensors after irradiation is the power balance inside the detector. If the cooling capacitance of the detector is not sufficient to remove the heat generated by the leakage current in the detector, this might result in a so called "thermal runaway". This phenomena is related to the fact that silicon is a semiconductor and as such has a negative temperature coefficient for the resistance. Hence a heating of the silicon due to leakage current increases the conductivity and therefore the leakage current. Due to this positive feedback, the detector does not reach a thermal equilibrium but rather tends to overheat. In order to ensure a proper operation, sufficient cooling of the sensor needs to be provided in order to keep it at a stable operating temperature. The cooling capacitance of the sensor considered here is just the cooling through natural thermal convection at various ambient temperatures. The size of the heat transfer coefficient h is estimated as described in the appendix A. The heat transfer coefficient for natural convection depends on the temperature difference, the size of the plate and the position on the plate. Averaged over the whole surface, it assumes a value of about 4-5 $\mathrm{W/(m^2{\cdot}K)}$ for an assumed temperature difference of $5\,^\circ C$ betwwen sensor and the ambient air[2]. This results in a cooling power of:

$$Q_{conv.} = h(T_{sensor} - T_{ambient}) \cdot A \cdot (T_{sensor} - T_{ambient}) \; ; \qquad (5)$$

where A is the sensor surface. Due to the relatively good heat conduction in Silicon with a thermal conductivity of approximately 100 $\mathrm{W/(m{\cdot}K)}$ it is assumed in this calculation that the power dissipation in the sensor results in a homogeneous temperature increase of the sensor. As can be seen in figure 8 the power dissipation in the sensors is well compensated by the power which can be removed by natural convective cooling for ambient temperatures inside the detector box somewhere between $5^\circ C$ and $10^\circ C$. For

[2]We are well aware of the fact that this number is not very well estabished, but this is the best (conservative) estimate we can get at the moment, resulting from test measurements of the ambient temperature reached in the detector box made in Zuerich[13], and temperature measurements on a IT-Ladder support structure in Lausanne[14]

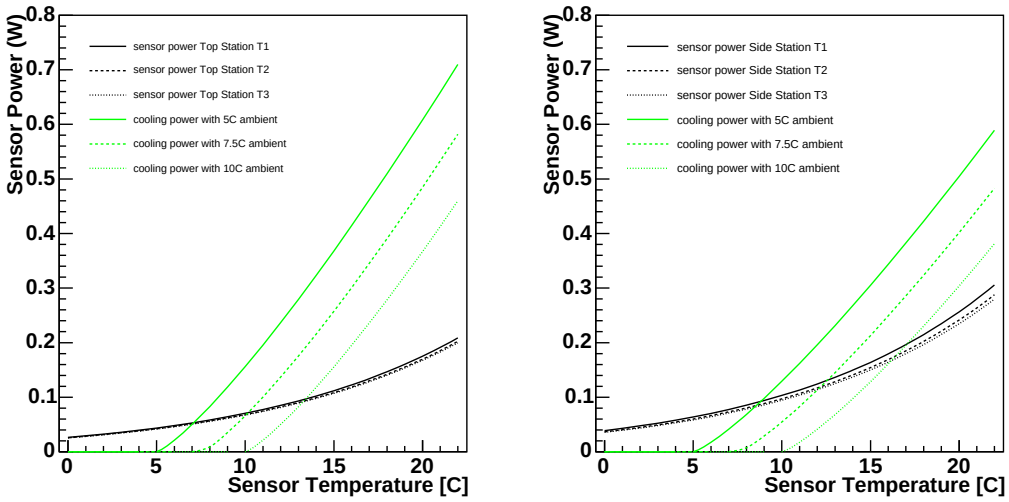

Figure 8: The power dissipation in the sensors closest to the beam-pipe after 10 years of operation as a function of the silicon bulk temperature for a bias voltage of 300V, together with the power removed from the sensors through free convection for given ambient temperatures.

these temperatures eventually there is an equillibrium sensor temperature at which the cooling power (green lines) are above the power generated in the sensors (black lines). However, the convective cooling will not enough anymore if a safety factor of two is included in the expected radiation dose as shown in the appendix B. In this case, the power dissipation in the sensors of the side box is just equal to the amount of power removed by convection given a ambient temperature of $5^\circ C$. For additional heat removal, either a forced convection would be needed, or a significant amount of heat needs to be removed via conduction within the CF-support. A simple calculation reveals the power which can be transported through the CF-support assuming the heat conduction coefficient of 200W/(m·K) measured for a similar support structure for the Inner Tracker TDR. The heat conduction is given by $Q = k \cdot A/L \cdot \Delta T$. With the carbon fibre sheet on the modules having a thickness of 0.2 mm, the module width being 78 mm and assuming for a rough estimate that all power is dissipated at the middle of the module at 110 mm distance from the balcony, this allows for a maximum of

$$200\mathrm{W}/(\mathrm{m}\cdot\mathrm{K})\cdot 0.2\mathrm{mm}\cdot 78\,\mathrm{mm}/110\,\mathrm{mm}\cdot 5\,\mathrm{K}\approx 0.15\,\mathrm{W} \qquad (6)$$

to be removed via the CF-support, given a temperature difference of maximum $5^\circ C$ within CF support similar to what is observed in [14]. This would then allow again the operation of the detector. It needs to be noted however, that this would require a perfect heat transfer between the silicon and the CF-support, which is certainly not the case for the small glue traces currently forseen to hold the sensors.

6 Summary

Given the radiation levels expected in the LHCb Inner Tracker the expected performance of the silicon detectors have been studied. The expected S/N for the choosen sensor thicknesses of 320 μm and 410 μm is sufficient for a large range of operating temperatures. For the choice of the p-on-n silicon microstrip detectors on standard float-zone silicon wafers with 4-9kΩ·m resistivity and 410 μm thickness, the depletion voltage after irradiation does not exceed 100 V. This allows for moderate operation voltages of maximal 300 V to ensure full charge collection. The design of the Inner Tracker [5] forsees a liquid cooling system which ensures an ambient temperature of about $5^\circ C$ in the detector box. At this temperature sufficient cooling of the sensors via natural convection is provided to compensate the power dissipation in the silicon.

A Determination of the convective heat transfer coefficient

Natural convection in a gas is due to buoyancy forces occurring for density variations in the gas, which simply causes to warm air to rise. Applying mass, momentum and energy conservation together with some simplifications, called the boundary layer approximations, the problem can be expressed mathematically. Different to forced flow a variable density has to be accounted to allow for fluid motion. The governing equations for mass, momentum and energy conservation are given as follows:

$$\frac{\partial u}{\partial x} + \frac{\partial v}{\partial y} = 0 \tag{7}$$

$$u\frac{\partial u}{\partial x} + v\frac{\partial v}{\partial y} = g\beta(T - T_\infty) + \nu\frac{\partial^2 u}{\partial y^2} \tag{8}$$

$$u\frac{\partial T}{\partial x} + v\frac{\partial T}{\partial y} = \alpha\frac{\partial^2 T}{\partial y^2} \tag{9}$$

As the variation in density is dependent on temperature the equations for momentum and energy conservation are no any longer decoupled, as it is the case for forced flow, and have to be solved simultaneously. A similarity solution to free convection from an isothermal vertical surface in an extensive quiescent medium has been obtained by Ostrach [15]. The averaged Nusselt number is given by equation 10.

$$\overline{Nu_L} = \frac{\overline{h}L}{k} = \frac{4}{3}\left(\frac{Gr_L}{4}\right)^{1/4} g(Pr) \tag{10}$$

$$g(Pr) = \frac{0.75Pr^{1/2}}{(0.609 + 1.221Pr^{1/2} + 1.238Pr)^{1/4}} \tag{11}$$

$$Gr_L = \frac{g\beta(T_s - T_\infty)L^3}{\nu^2}, Pr = \frac{\nu}{\alpha} \tag{12}$$

$$\beta = -\frac{1}{\rho}\left(\frac{\partial\rho}{\partial T}_p\right) = \frac{1}{\rho}\frac{p}{RT^2} = \frac{1}{T} \tag{13}$$

where the Nusselt number is an universal function of Gr (Grashof number), Pr (Prandtl number) and the characteristic length of a prescribed geometry. The Grashof number indicates the ratio of the buoyancy force to the viscous force acting on the fluid, comparable to the Reynolds number in forced flow. The Prandtl number provides a measure of the relative effectiveness of momentum and energy transport by diffusion in the velocity and thermal boundary layers respectively. The volumetric thermal expansion coefficient β is the inverse temperature for ideal gases, as the density $\rho = \frac{p}{RT}$. In the following the values for the above mentioned constants are given in brackets for 300 K: kinematic viscosity ($\nu = 15.89 \cdot 10^{-6} m^2/s$), thermal diffusity ($\alpha = 22.5 \cdot 10^{-6} m^2/s$) and g stands for the gravitational acceleration ($9.81 m/s^2$) [21].

As seen in equation 10 the average heat convection coefficient can be derived by multiplying the Nusselt number with the thermal conductivity at the boundary and dividing by the characteristic length. Multiplying the Grashof number with the Prandtl number the Rayleigh number is obtained, which gives a measure of the stability of the flow. Although turbulences are appreciable for enhanced heat transfer, the conditions in the Inner Tracker are such that the Rayleigh number is far under-critical and laminar flow has to be assumed. The dependence of the Rayleigh number on surface and ambient temperature is expressed in formula 14.

$$Ra_{x,c} = Gr_{x,c}Pr = \frac{g\beta(T_s - T_\infty)x^3}{\nu\alpha} \approx 10^9 \tag{14}$$

Empirical correlations for the Nusselt number can be found in [16, 17, 18]. A general form is given in equation 15, where for a laminar flow on a vertical plate C= 0.59 and n=1/4.

$$\overline{Nu_L} = \frac{\overline{h}L}{k} = C\ Ra_L^n \tag{15}$$

A correlation that may be applied over the entire range of Rayleigh numbers has been recommended by Churchill and Chu [19] and is given in 16.

$$\overline{Nu_L} = (0.825 + \frac{0.387Ra_L^{1/6}}{[1 + (0.492/Pr)^{9/16}]^{8/27}})^2 \tag{16}$$

Although equation 16 is suitable for most engineering calculations, slightly better accuracy may be obtained for laminar flow by using [19] equation 17.

$$\overline{Nu_L} = 0.68 + \frac{0.670Ra_L^{1/4}}{[1 + (0.492/Pr)^{9/16}]^{4/9}} \tag{17}$$

Using these models, the heat conduction coefficient on a vertical plane like our silicon modules has been calculated assuming the sensors to be an isothermal plate. Uncertainties in these calculations are quoted in the literature to be of the order of 25 %. A detailed discussion of constant heat flux as boundary condition is provided by Churchill [20].

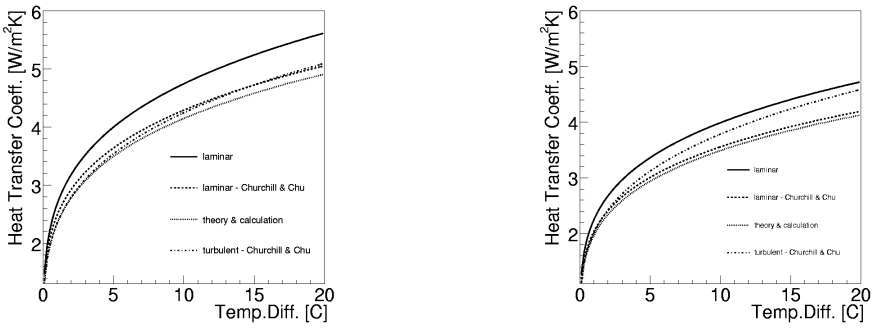

Figure 9: Averaged heat transfer coefficient for the single sensor module (left) and the double sensor module (right).

The two plots in figure 9 show the dependence of the various models on the temperature difference between surface and ambient. On the top the characteristic length was put as 11 cm, corresponding to the one-sensor module and on the bottom 22 cm for the two-sensor module. Comparing the plots one can see that the average heat transfer coefficient is slightly smaller for longer modules. It is worth mentioning that the empirical obtained values by Churchill and Chu are very close to the theoretically derived ones. The model provided by Churchill, valid for the whole range of Rayleigh numbers, is increasing significantly faster as the one valid for lower Rayleigh numbers when looking on the two-sensor module. This is due to the fact that this model has to account for turbulences as well, as mentioned above.

Studies have been as well performed on the thickness of the boundary layer. It could be seen that the spacing between the various modules does not affect the heat convection significantly. After a spacing larger than 2 cm is reached, the changes of the averaged heat transfer coefficient are negligible. A study on forced flow shows that the average heat transfer coefficient is around $10W/m^2K$ for a flow of around 1 m/s. This value decreases rapidly with decreasing flow. Such that for a one-sensor module the dissipated power is around 0.3 Watts per 10 K temperature difference between surface and ambient, assuming a flow of 5cm/s. The latter calculation neglects all effects of natural convection, resulting in a zero heat transfer for zero flow velocity and hence doesn't represent a good model for small velocities.

B S/N and energy balance if expected radiation is doubled

In this section, the expected detector performance in terms of the S/N and the energy balance for the cooling of the silicon sensors are shown in case of a safety factor included in the assumed radiation dose.

It can clearly be seen, that the expected detector performance also after twice the nominal radiation dose, no problems are to be expected in terms

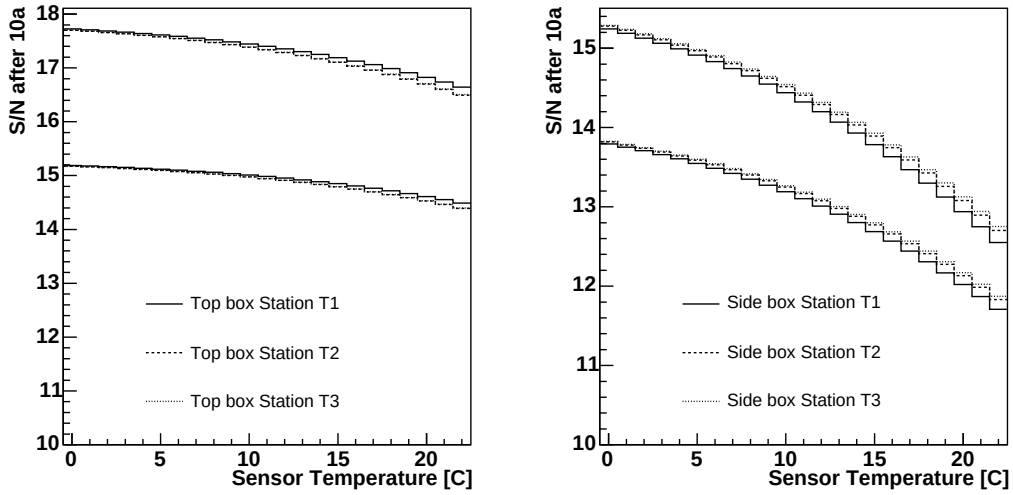

Figure 10: The expected S/N performance of the detector dependent on the operating temperature after 10 years of operation, including a safety factor of 2 in the expected radiation dose. The upper plot corresponds to the optimistic approach using the lab measurements of the Beetle performance, while the lower curves correspond to the values closer to the test-beam.

of the achieved S/N in the silicon detectors. The total radiation dose would in this case be of the order of $2{\cdot}10^{13}$ 1 MeV Neutron equivalent /cm^2, which is still a relatively moderate dose. However the power dissipation due to the increased leakage current in this case rises considerably above the power which can be removed by natural convection given an ambient temperature in the box of $5\,^\circ C$. In this case, a good thermal contact between the Silicon and the CF-support is essential in order to provide the additional cooling via the heat conduction.

References

[1] LHCb Collaboration: *LHCb Inner Tracker*, CERN/LHCC 2002-029.

[2] LHCb Collaboration: *LHCb Reoptimized Detector, Design and Performance*, CERN/LHCC 2003-030.

[3] http://www.fluka.org

[4] G. Corti and L. Shekhtman, *Radiation Background in the LHCb Experiment*, LHCb note 2003-083.

[5] P. Fauland, R .Frei, J.Ph. Hertig, A. Perrin, M.T. Tran,J. van Hunen, K. Vervink, H. Voss,*Mechanics for the LHCb Inner Tracker*, LHCb-note 2004-108.

[6] M. Moll *et al.*, Nucl. Instr. Meth. **A426** (1999) 87.

[7] F. Lehner, C. Lois, H. Voss, *Measurements on irradiated silicon sensor prototypes for the Inner Tracker of LHCb*, LHCb-note 2004-108.

[8] M. Moll, PhD thesis, DESY-THESIS-1999-040.

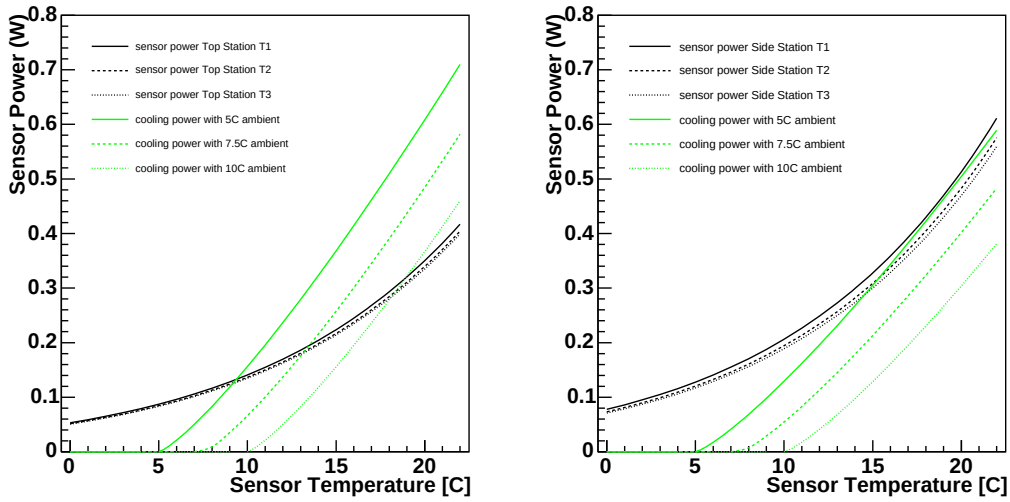

Figure 11: The power dissipation in the sensors closest to the beam-pipe after 10 years of operation with a safety factor of two, as a function of the silicon bulk temperature for a bias voltage of 300V, together with the power removed from the sensors through free convection for given ambient temperatures.

[9] S. Baribant *et al.*, Nucl. Instr. Meth. **A485** (2002) 343.

[10] M. Agari et al:*Testbeam measurements on prototype ladders for the LHCb TT station and Inner Tracker*, LHCb note 2003-082.

[11] J. Gassner, M. Needham, O. Steinkamp:*Layout and Performance of the LHCb TT station*, LHCb note 2003-140.

[12] N.v. Bakel *et al.*, *The Beetle Reference Manual - Chip version 1.3, 1.4 and 1.5*, http://wwwasic.kip.uni-heidelberg.de/lhcb/Publications/BeetleRefMan_v1_3.pdf, LHCb note 2005-105.

[13] K. Bösiger, F. Lehner, S. Steiner and S. Strässle, *Design, Construction and Thermal Measurements on a Detector Box for the Inner Tracker of the LHCb Experiment*, LHCb note 2002-059.

[14] R.J. Frei, J.-P. Hertig, S. Jimnez-Otero, M.T. Tran, H. Voss: *Thermal and mechanical studies of the carbon fibre support for the LHCb Inner Tracker sensors*, LHCb note 2002-060.

[15] Ostrach, S.: *An Analysis of Laminar Free Convection Flow and Heat Transfer About a Flat Plate Parallel to the Direction of the Generating Body Force*, National Advisory Committee for Aeronautics, Report 1111, 1953.

[16] McAdams, W.H.: *Heat Transmission*, 3rd ed., McGraw-Hill, New York, 1954, Chap.7.

[17] Warner, C.Y.:*An Experimental Investigation of Turbulent Natural Convection in Air at Low Pressure for a Vertical Heated Flat Plate*, Int.J.Hat Mass Transfer, 11, 397, 1968.

[18] Bayley, F.J.? *Analysis of Turbulent Free Convection Heat Transfer*, Proc. Inst. Mech. Eng., 169, 361, 1955.

[19] Churchill, S.W., and Chu, H.H.S.? *Correlating Equations for Laminar and Turbulent Free Convection from a Vertical Plate*, Int.J.Heat Mass Fransfer, 18, 1323,1975.

[20] Churchill, S.W.:*Free Convection Around Immersed Bodies* in E.U. Schlünder, Ed.-in-Chief, Heat Exchange Design Handbook, Section 2.5.7, Hemisphere Publishing, New York, 1983.

[21] Incoprera F.P.and Witt de, D.P.: *Fundamentals of Heat and Mass Transfer*,5th ed.,John Wiley & Sons, 2002.